scientific reports

Check for updates

OPEN

Crystal growth of clathrate hydrate formed with $H_2 + CO_2$ mixed gas and tetrahydropyran

Meku Maruyama, Riku Matsuura & Ryo Ohmura✉

Hydrate-based gas separation technology is applicable to the CO_2 capture and storage from synthesis gas mixture generated through gasification of fuel sources including biomass. This paper reports visual observations of crystal growth dynamics and crystal morphology of hydrate formed in the $H_2 + CO_2$ + tetrahydropyran (THP) + water system with a target for developing the hydrate-based CO_2 separation process design. Experiments were conducted at a temperature range of 279.5–284.9 K under the pressure of 4.9–5.3 MPa. To simulate the synthesis gas, gas composition in the gas phase was maintained around H_2:CO_2 = 0.6:0.4 in mole fraction. Hydrate crystals were formed and extended along the THP/water interface. After the complete coverage of the interface to shape a polycrystalline shell, hydrate crystals continued to grow further into the bulk of liquid water. The individual crystals were identified as hexagonal, tetragonal and other polygonal-shaped formations. The crystal growth rate and the crystal size varied depending on thermodynamic conditions. Implications from the obtained results for the arrangement of operating conditions at the hydrate formation-, transportation-, and dissociation processes are discussed.

The elevation of CO_2 emissions in the atmosphere is a central, common concern worldwide both in environmental and political manners. Various industrial processes discharge CO_2-including synthesis gas, which entails corresponding CO_2 capture and storage (CCS) technique. One approach is "pre-combustion" process, through which CO_2 is captured prior to the fuel combustion in power plants. This pre-combustion capture can be applied to separate CO_2 from syngas mixture generated through gasification of fuel sources (e.g., coal, natural gas, and biomass). Particularly, the development of biomass energy may promote the reduction of greenhouse gas emissions[1–3]. Through biomass gasification processes, syngas mixture of H_2, CO_2, CH_4, CO is produced[4,5]. After water–gas-shift reaction, this syngas mixture can subsequently be converted into $H_2 + CO_2$ gas mixture[6], which requires CCS process. For this purpose, an emerging method is under development, a process utilizing clathrate hydrate crystallization[7].

Clathrate hydrates (hydrates) are crystalline inclusion solids of cage-like hydrogen-bonded host water molecules encaging guest molecules of gaseous or organic compounds, which form under definite thermodynamic conditions. Hydrates have several unique properties including large capacity of gas storage[8–10] and guest compound selectivity[11,12], both of which render an undertaking of hydrate-based gas separation feasible. In addition, any hydrate-based industrial application is harmless to the environment, for the main constituent of hydrate is water molecules, which produces no toxic chemicals during the formation, transportation and decomposition process.

As an alternative CCS method to two major existing technologies, namely chemical absorption[13,14], which can be toxic and harmful to the ecosystem, and membrane separation[15,16] necessitating frequent maintenance and accordingly high cost, hydrate-based gas separation is one burgeoning technology. Moreover, CO_2 capturing by hydrate-based gas separation has comparable to or even lower energy consumption than chemical absorption or membrane separation[17]. Previous studies have shown a great amount of potential of this line; various experiments have been conducted using batch, semi-batch type and continuous separation methods[17–20]. Among these three methods of separation, continuous separation is best suited for industrial use[20]; while batch-type operations involve several sets of reactors to produce purified gas continuously, in the continuous operation, a series of procedures from hydrate formation via discharge of hydrate slurry to hydrate dissociation suffice a single set of reactors and all these procedures are performed concurrently. Therefore, the capital investment for plant construction and operating costs are to be lessened when introducing the continuous separation system. Horii and Ohmura[20] performed continuous CO_2-separation experiments in the $H_2 + CO_2$ + water and

Department of Mechanical Engineering, Keio University, 3-14-1 Hiyoshi, Kohoku-ku, Yokohama, Kanagawa 223-8522, Japan. ✉email: rohmura@mech.keio.ac.jp

Authors	System	Feed gas composition by mole fraction	Experimental condition		Results		Ref
			Temperature (K)	Pressure (MPa)	H_2:CO_2 mole fraction in the gas phase	H_2:CO_2 mole fraction in the slurry phase	
Horii and Ohmura	$H_2 + CO_2$ + water	H_2:CO_2 = 0.6:0.4	271.8	7.0	0.87:0.13	0.00:1.00	[20]
Horii and Ohmura	$H_2 + CO_2$ + TBAB + water	H_2:CO_2 = 0.6:0.4	277.4	5.0	0.81:0.19	0.18:0.82	[20]
Kiyokawa et al	$H_2 + CO_2$ + THP + water	H_2:CO_2 = 0.6:0.4	277.7	5.0	0.92:0.08	0.00:1.00	[17]

Table 1. Summary of experimental results of continuous CO_2-separation studies.

$H_2 + CO_2$ + tetra-*n*-butylammonium bromide (TBAB) + water systems. Kiyokawa et al.[17] reported an improved CO_2-separation performance in the system of $H_2 + CO_2$ + tetrahydropyran (THP) + water. THP is one of the large-molecule guest compounds (LMGC) with water solubility to the hydrate forming system, working as a thermodynamic promoter to moderate the equilibrium pressure. Table 1 summarizes mole fractions of H_2 and CO_2 after repetitions of operation for 38 h in the gas phase and in the hydrate-slurry phase from these experimental studies. As these results demonstrate, the separation process adding THP in the system matches a practical operation most advantageously of the three systems, because of the fact that the CO_2 mole fraction in the gas phase reaches the lowest value, that is, separation efficiency of this system is the highest, and that the H_2 mole fraction in the slurry phase falls to 0.00, to rephrase it, purified CO_2 can be obtained through the capture and storage process.

For the design of the hydrate formation-, transportation- and dissociation processes to realize, hydrate crystal growth dynamics and crystal morphology need to be clarified. As previous studies have shown, hydrates are usually formed at the interface or in the bulk of the water phase[21–25]. Therefore, one method to multiply the amount of hydrate formation is the expansion of the interfacial area. Crystal morphology, which indicates crystal shape and size, affects dehydration and transportation energy efficiencies of hydrate slurry; when hydrate crystals are small in size, the pressure loss during the transportation of hydrate slurry increases and the dehydration efficiency of the slurry decreases[26]. In the dissociation process, hydrate crystals with large surface areas per unit volume such as dendritic crystals decompose promptly owing to the increase of the overall rate of heat transfer, whilst hydrate crystals with small surface areas such as polygonal crystals remain undissociated for a longer period of time. Thus, understanding of crystal growth dynamics and crystal morphology forms the foundation of hydrate-based gas separation technology.

Previous experimental studies have revealed that crystal growth dynamics and crystal morphology of hydrate are resultant from the characteristics of the guest compounds and thermodynamic conditions of the hydrate-forming system. Ohmura et al.[27] performed crystal growth observations for CO_2 hydrate that covers the CO_2-water interface and forms a film. They demonstrated that the crystal morphology ranges from dendritic to skeletal or polyhedral depending on thermodynamic conditions. Ueno et al.[28] observed $CH_4 + CO_2$ hydrate crystal growth at the gas/liquid interface and in liquid water. They suggested that the crystal morphology is determined by the guest composition in the liquid phase. Akiba et al.[29] performed crystal growth observations on the surface of a liquid droplet of TBAB aqueous solution exposed to CO_2 gas. Ozawa and Ohmura[30] observed the formation and growth of methane + THP hydrate crystals, clarifying that the morphology varies from pyramidal to an "oligo-polygon" depending on thermodynamic conditions. However, there is no report of crystal growth in a system with $H_2 + CO_2$ gas in preceding studies.

In the present work, visual observations of crystal growth of hydrate formed with $H_2 + CO_2$ mixed gas, liquid THP and liquid water were conducted under different thermodynamic conditions. This study draws a bead on contributing to the industrial utilization of hydrate-based H_2/CO_2 separation with a crystallographic approach.

Results and discussion

Crystal growth dynamics. We conducted several experimental runs under each experimental condition for the confirmation of reproducibility and demonstrate the representative results here. THP and water are partially soluble. Therefore, partial solubility between THP and water leads to phase separation (liquid THP-liquid water). The mutual solubility data of THP and water, reported by Stephenson[31], are demonstrated in Table S1. The mole fraction of THP in the aqueous phase is calculated to be $1 - 0.112 = 0.888$. The mole fraction of water in the aqueous phase is calculated to be $1 - 0.023 = 0.977$. The measured equilibrium conditions, which were obtained experimentally in the present study, and the corresponding gas compositions in each experimental system are summarized in Table 2. We defined the subcooling temperature ΔT_{sub} as a difference between the phase equilibrium temperature of the hydrate-forming system and the experimental temperature ($\Delta T_{sub} \equiv T_{eq} - T_{ex}$), which is an index of driving force for the crystal growth. Crystal growth observations were conducted under several ΔT_{sub} conditions, namely, from $\Delta T_{sub} = 1.3$ K to $\Delta T_{sub} = 7.1$ K. We determined the experimental conditions as to prevent the formation of $H_2 + CO_2$ binary hydrate.

Observations of hydrate crystals on a water droplet are presented in Figs. 1, 2 and 3. Figure 1 shows sequential images of growing process of $H_2 + CO_2$ + THP hydrate at $T_{ex} = 284.2$ K, $\Delta T_{sub} = 1.3$ K, $P = 5.00$ MPa. We determined $t = 0$ as the time when the nucleation of hydrate crystals was first identified visually. The hydrate nucleation was observed at the THP/water interface (Fig. 1a). As time proceeded, this nucleated hydrate crystal grew to form a polygonal plate along the THP/water interface (Fig. 1b). Subsequently, newly nucleated crystals were observed on the edge of the existing crystal plate (Fig. 1c). These hydrate crystals continued to grow and gradually covered the entire THP/water interface (Fig. 1d–f). After this time ($t = 97$ min), no noticeable further hydrate crystal growth was observed.

Figure number	Equilibrium condition		H_2:CO_2 gas composition (mole fraction)
	T_{eq} (K)	P (MPa)	
1, 2	285.5	5.00	0.55:0.45
3	286.6	5.00	0.55:0.45
4	287.1	5.42	0.55:0.45
5	286.2	5.08	0.65:0.35

Table 2. Equilibrium conditions and gas compositions in each experimental system.

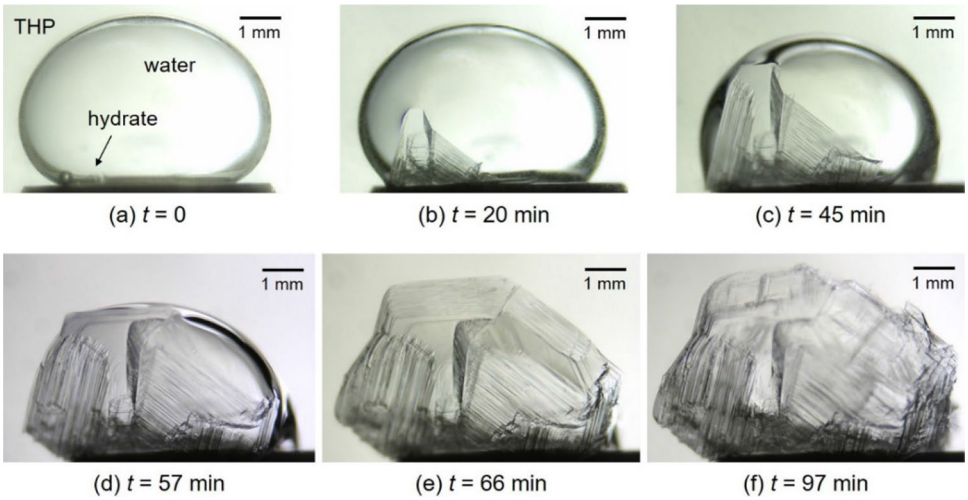

Figure 1. Sequential images of $H_2 + CO_2 + THP$ hydrate growing on a water droplet at $T_{ex} = 284.2$ K, $\Delta T_{sub} = 1.3$ K, $P = 5.00$ MPa. The gas composition was H_2:CO_2 = 0.55:0.45 in mole fraction. The elapsed time after the hydrate nucleation is indicated below each image.

Although the time to hydrate formation process in this laboratory-scale system is quite long (97 min) for engineering practice, technical improvements could help shorten the time. For instance, installation of a process using micro-bubbles with a tubular reactor could enhance the hydrate formation rate 50 times[32]. In addition, hydrate nucleation rate could be improved with the 10^3 of the size of a hydrate forming reactor.

Figure 2 shows sequential images of growing process of $H_2 + CO_2 + THP$ hydrate at $T_{ex} = 283.0$ K, $\Delta T_{sub} = 2.5$ K, $P = 5.00$ MPa. As recognized on the lower left of the images, hydrate crystals were nucleated and extended along the THP/water interface (Fig. 2a–c). At a subsequent time to the first nucleation, another nucleation was observed as recognized on the lower right of the image (Fig. 2b). These two lumps of hydrate crystals extended separately until they grew fully to collide, covering the entire droplet surface (Fig. 2c–e).

Figure 3 shows sequential images of growing process of $H_2 + CO_2 + THP$ hydrate at $T_{ex} = 282.1$ K, $\Delta T_{sub} = 4.5$ K, $P = 4.95$ MPa. At this raised ΔT_{sub}, hydrate crystals grew and covered the THP/water interface rapidly after the first nucleation. As recognized in comparison of Figs. 1, 2 and 3, the time needed for the complete coverage of the droplet surface varies with the subcooling; when ΔT_{sub} is lowered, longer time is required. This difference of the elapsed time would be attributed to the difference of the hydrate nucleation rate and the crystal growth rate, both of which are affected by the driving force for crystal growth related to the magnitude of ΔT_{sub}.

Observations of hydrate crystals in a two-layer pool are presented in Fig. 4. Figure 4 shows sequential images of growing process of $H_2 + CO_2 + THP$ hydrate at $T_{ex} = 282.0$ K, $\Delta T_{sub} = 5.1$ K, $P = 5.30$ MPa. At $t = 0$, the hydrate nucleation was observed at the THP/water interface (Fig. 4a). This hydrate grain grew to form a pyramid (Fig. 4b) and gradually spread along the interface (Fig. 4c). After the complete coverage, the pyramidal crystal grew further into the bulk of water. Concurrently, minute hydrate grains sprouted up from the surface of the pyramidal crystal (Fig. 4d). These hydrate grains grew to form polygonal sheets, some of which detached from the surface (Fig. 4e). The lump of hydrate crystals covering the interface and the newly formed polygonal crystals grew larger (Fig. 4f).

This crystal growth behavior of hydrate formed in the liquid bulk exposed to $H_2 + CO_2$ is different from that of hydrate formed with CH_4; in the $CH_4 + THP +$ water system, it is reported that hydrate is detached from the THP/water interface after the formation at the interface. Eventually, hydrate crystals which have been detached from the interface accumulate in the bulk of liquid water, without covering the THP/water interface[30]. In contrast, hydrate formed in this study promptly spread the entire THP/water interface before detaching (Fig. 4c). Therefore, it is inferred that the crystal growth rate of $H_2 + CO_2 + THP$ hydrate at the interface is greater than that of $CH_4 + THP$ hydrate. One possible factor of this difference would be the gap of the interfacial free energies. The interfacial free energy in the $CO_2 +$ water system could be smaller than that in the $CH_4 +$ water system,

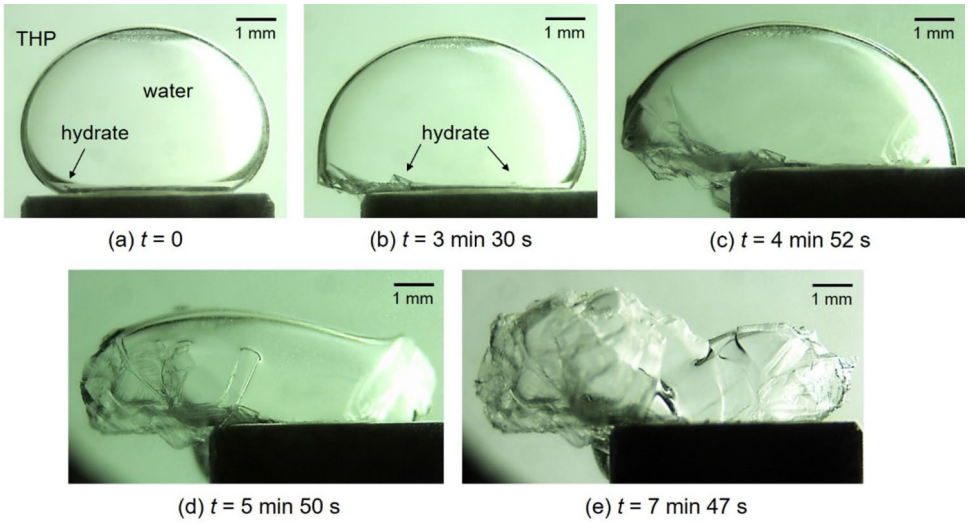

Figure 2. Sequential images of $H_2 + CO_2 + THP$ hydrate growing on a water droplet at $T_{ex} = 283.0$ K, $\Delta T_{sub} = 2.5$ K, $P = 5.00$ MPa. The gas composition was H_2:$CO_2 = 0.55$:0.45 in mole fraction. The elapsed time after the hydrate nucleation is indicated below each image.

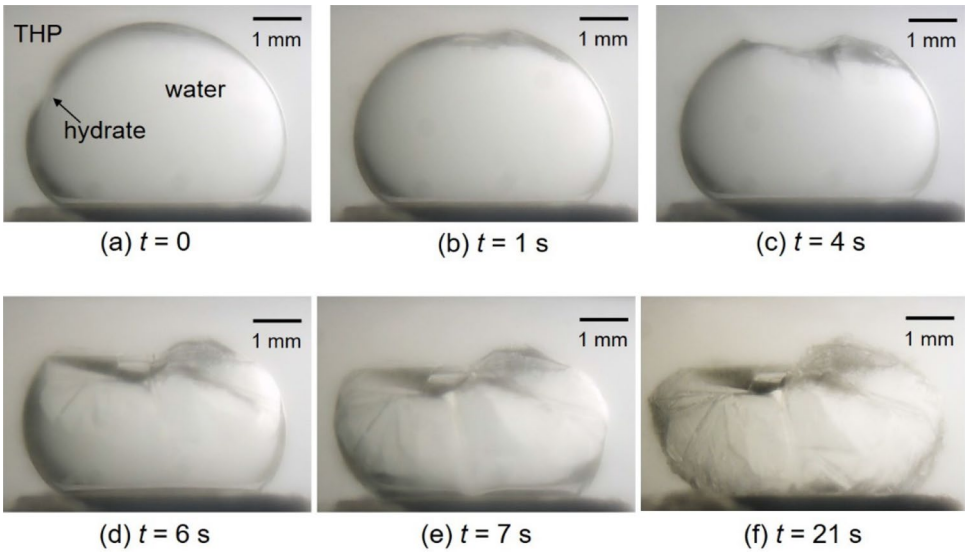

Figure 3. Sequential images of $H_2 + CO_2 + THP$ hydrate growing on a water droplet at $T_{ex} = 282.1$ K, $\Delta T_{sub} = 4.5$ K, $P = 4.95$ MPa. The gas composition was H_2:$CO_2 = 0.55$:0.45 in mole fraction. The elapsed time after the hydrate nucleation is indicated below each image.

resulting from the larger solubility of CO_2 in water. Accordingly, the critical radius of $H_2 + CO_2 + THP$ hydrate is considered smaller than that of $CH_4 + THP$ hydrate, both of the hydrates being structure II, which results in the increase of the nucleation rate and thereby the improvement of the formation rate.

Crystal morphology. We focus on hydrate single crystals formed at different levels of ΔT_{sub}. Figure 5 shows temporal development of hydrate single crystals growing in the bulk of liquid water at $\Delta T_{sub} = 4.8$ K under $P = 5.08$ MPa. Sequential images of enlarged part from Fig. 5a (enclosed by blue lines) are demonstrated in Fig. 5b–e. As recognized in Fig. 5b–e, the formation and growth of polygonal crystal plates were observed. Their high transparency would indicate that each plate was a hydrate single crystal. One crystal platelet grew to be hexagonal (emphasized by red lines) and another platelet formed into tetragonal (emphasized by green lines). These configurations may be attributed to the growing habit of hydrate crystals; it is reported that single crystals of cubic structure II hydrates grow to be octahedral or thin polygonal platelets[33–36]. Therefore, the observed hexagonal crystal plate exhibits a section parallel to the {111} plane of an octahedron. On the other hand, the observed tetragonal crystal plate is the "skeletal 60° plate" that Knight and Rider described[36]. According to their study, skeletal 60° plates of structure II hydrates appear when ΔT_{sub} are above 3 or 4 K in the THP + water sys-

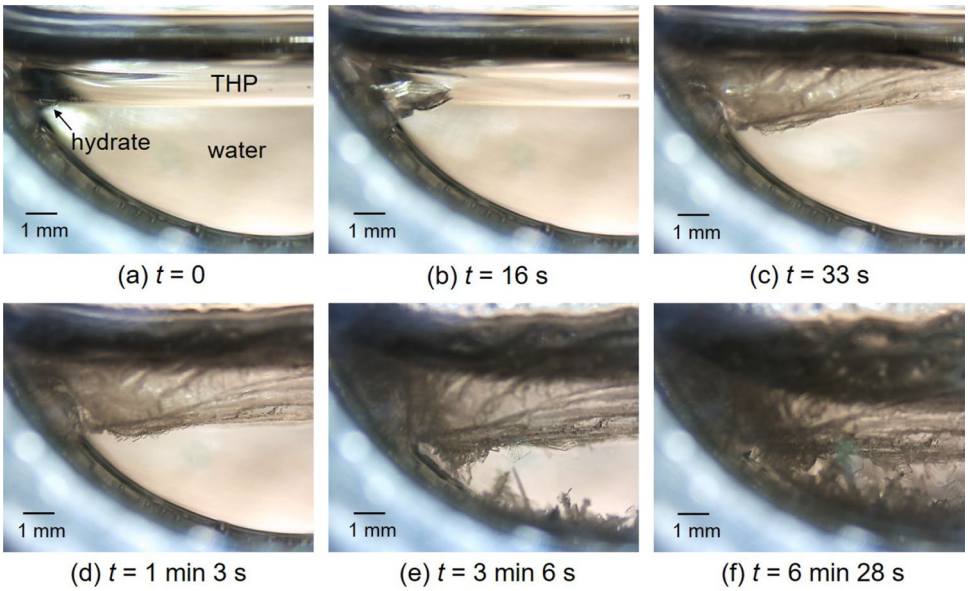

Figure 4. Sequential images of $H_2 + CO_2 +$ THP hydrate growing in the liquid bulk at $T_{ex} = 282.0$ K, $\Delta T_{sub} = 5.1$ K, $P = 5.30$ MPa. The gas composition was H_2:$CO_2 = 0.55$:0.45 in mole fraction. The elapsed time after the hydrate nucleation is indicated below each image.

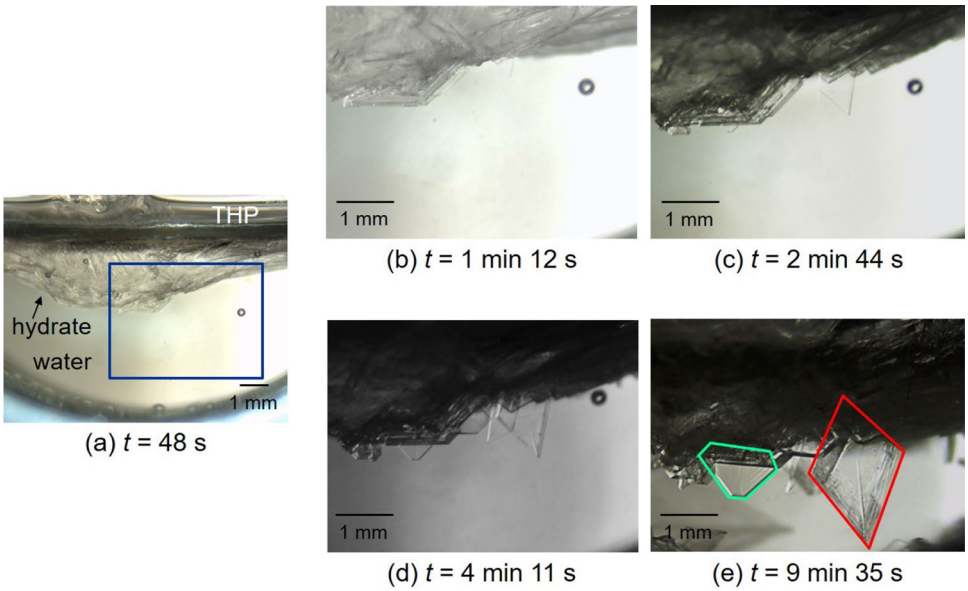

Figure 5. Sequential close-up images of $H_2 + CO_2 +$ THP hydrate crystal plates growing in the bulk of liquid water at $\Delta T_{sub} = 4.8$ K under $P = 5.08$ MPa. The gas composition was H_2:$CO_2 = 0.65$:0.35 in mole fraction. The elapsed time after the hydrate nucleation is indicated below each image.

tem. This configuration is another typical form of structure II hydrates[34]. Although the mechanism of forming skeletal 60° plates is hard to explain in a crystallographic manner and is not revealed in the study by Knight and Rider[36], visual observations of this study agree with the previous study. Thus, the observations would attest the fact that $H_2 + CO_2 +$ THP hydrate is structure II hydate[37].

Figure 6 presents arrangement of morphology of hydrate crystal plates growing on a water droplet based on ΔT_{sub}, where representative individual crystals are enclosed by red lines. At all ΔT_{sub}, polygonal crystals were observed. The polygonal shape of plates may be a plane of an octahedron or demonstrate thin platelets. The difference depending on ΔT_{sub} was recognized in size of plates; as ΔT_{sub} rises, the side length of a single crystal plate decreases. Previous studies indicated that hydrate crystal morphology depends on the balance between the crystal nucleation rate and the crystal growth rate. When ΔT_{sub} increases, the nucleation rate rises and the

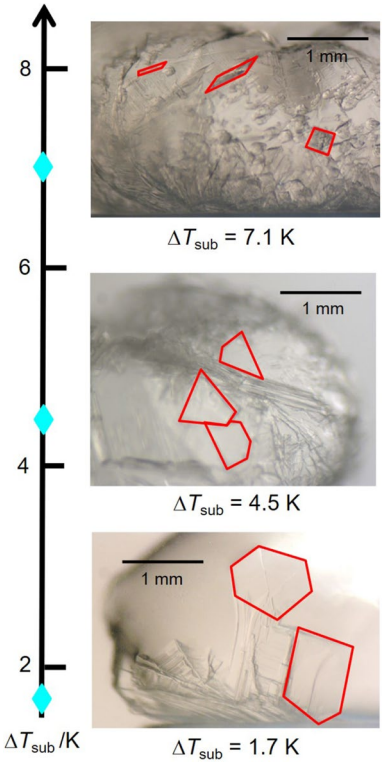

Figure 6. Arrangement of crystal morphology of $H_2 + CO_2 +$ THP hydrate growing on a water droplet based on ΔT_{sub}.

number of crystals increases. Subsequently, growth of individual crystals is restricted since contact among crystals intensifies. Consequently, the size of crystals becomes small.

Implication for industrial utilization. All of the experiments were conducted under the $H_2 + CO_2$ gas composition generally in consistent with that of systhesis gas produced from fuel sources, which is H_2:CO_2 = 0.6:0.4 in mole fraction. Therefore, the observations are to be applied to the hydrate-based CO_2 separation process design. As described in the section **Crystal Growth Dynamics**, the time required for complete hydrate growth is shortened as ΔT_{sub} increases. This result concludes that the hydrate growth rate could be improved by the operation at a low temperature. On the other hand, resulted from the section **Crystal Morphology**, during the transportation process from the hydrate forming reactor to the hydrate dissociation vessel, smaller ΔT_{sub} is suitable. When the crystal size is large, the viscosity of hydrate slurry would decrease as derived from the rheological behavior, and the pressure loss becomes smaller[26]. Considering the dissociation process, larger ΔT_{sub} is appropriate. The surface area of hydrate crystals per unit volume increases as the size of polygonal crystals becomes smaller, which leads to enhanced heat and mass transfer. To determine the appropriate operating conditions, optimal value can be selected as a compromise.

From the obtained results suggesting that $H_2 + CO_2 +$ THP hydrate is ready to form at the THP/water interface, it is concluded that hydrate formation methods with constant contact between THP and water would enhance the formation rate. Moreover, the observed successive water conversion to hydrate may represent sufficient crystal growth for the transportation process of hydrate slurry. For the continuous separation, water conversion ratio of approximately 10 ~ 20% is desirable to keep the fluidity of slurry.

The crystal morphology of $H_2 + CO_2 +$ THP hydrate corresponds to those of other structure II hydrates observed in previous studies. Therefore, it is considered that the knowledge of structure II hydrate crystal growth that has been previously obtained can be applied to the hydrate-based separation process design.

Ricaurte et al.[11] and Delroisse et al.[38] reported that the combination of surfactant and organic compound enhances the water conversion into hydrate and thereby improves the CO_2 separation efficiency in the batch system. Therefore, a combination of kinetic and thermodynamic promoters would provide a novel insight into hydrate-based continuous separation.

Methods

The fluid samples used in the experiment were liquid tetrahydropyran (99 mass %, Aldrich Chemical Co.), $H_2 + CO_2$ mixed gas (CO_2 certified purity of 39.7 vol %, Taiyo Nippon Sanso Co.), carbon dioxide gas (99.5 vol %, Taiyo Nippon Sanso Co.) and deionized, distilled water. Figure 7 shows the schematic diagram of the experimental apparatus. The test section is a stainless-steel cylindrical vessel with a pair of flange-type glass windows.

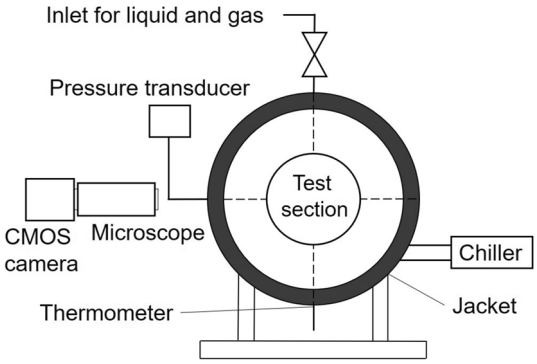

Figure 7. Schematic diagram of the experimental apparatus.

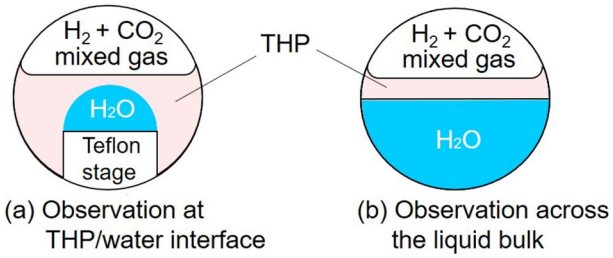

Figure 8. Schematic diagram of the test section.

The inner space of the test section is 25 mm in diameter and 20 mm in axial length. Figure 8a illustrates a frame format of the test section to observe hydrate at the liquid THP / liquid water interface. In this case, a cylindrical Teflon stage 6 mm in diameter was installed to hold a water droplet. Figure 8b describes a diagram of the test section to observe hydrate growing across the liquid bulk. The temperature inside the test section T_{ex} was controlled by circulating an ethylene glycol solution through a brass jacket covering the reactor, and measured by a Pt-resistance thermometer inserted from the undersurface of the reactor into the bulk of the liquid phase. The pressure inside the test section P was measured by a strain gauge pressure transducer. The estimated uncertainties of measurements were ± 0.2 K in temperature and ± 0.05 MPa in pressure. The formation and growth of hydrate crystals were observed and recorded using a CMOS camera (Aprolink Co.) and a microscope (Edmund Optics Co.).

The first process of the experimental procedure was the injection of liquid samples into the test section. For the observation of hydrate at the liquid THP/liquid water interface (see Fig. 8a), 4.0 cm^3 of liquid THP was injected into the test section. Subsequently, a water droplet was placed on the Teflon stage, entirely immersed in the liquid THP phase. For the observation of hydrate growing across the liquid bulk (see Fig. 8b), 2.5 cm^3 of liquid water and 0.5 cm^3 of liquid THP were injected into the test section to form a two-layer pool. The air in the test section was then replaced with CO_2 gas at about 1.0 MPa by repeating the process of pressurization and evacuation. $H_2 + CO_2$ mixed gas was charged in this vessel to approximately 5.5 MPa. Gases (primarily CO_2) dissolved in liquids and P was settled to nearly 5.0 MPa in a steady state. After the completion of these procedures, T was lowered to approximately 270 K to form hydrate (and simultaniously ice). T was then increased stepwise by 0.1 K to experimentally determine the phase equilibrium temperature of the hydrate-forming system T_{eq} and to dissociate crystals. At each step, when no remarkable change of hydrate dissociation was observed within 10 min, T was increased. The temperature at which hydrate crystals were visually observed to dissociate rapidly was determined to be the equilibrium temperature T_{eq}. After the dissociation of all hydrate crystals, T was set to the experimental temperature of crystal formation T_{ex} to form hydrate and to observe the hydrate formation and growth. After the observation, the $H_2 + CO_2$ gas composition was analyzed by a gas chromatograph. The equilibrium temperature measurement and the measurement of gas composition were conducted for each experimental run.

T_{ex} was set in the range from 279.5 to 284.9 K and P was in the range from 4.9 to 5.3 MPa. The reduction of system pressure resulted from the growth process of hydrate was less than 0.05 MPa, which is smaller than the uncertainty of pressure measurements.

Data availability

The datasets generated during and/or analysed during the current study are available from the corresponding author on reasonable request.

Received: 5 March 2021; Accepted: 17 May 2021
Published online: 31 May 2021

References

1. Field, C. B., Campbell, J. E. & Lobell, D. B. Biomass energy: the scale of the potential resource. *Trends Ecol. Evol.* **23**(2), 65–72 (2008).
2. Mao, G. *et al.* Research on biomass energy and environment from the past to the future: a bibliometric analysis. *Sci. Total Environ.* **635**, 1081–1090 (2018).
3. Nikola, B. *et al.* Evaluation of Croatian agricultural solid biomass energy potential. *Renew. Sustain. Energy Rev.* **93**, 225–230 (2018).
4. Fan, X., Yang, L. & Jiang, J. Experimental study on industrial-scale CFB biomass gasification. *Renew. Energy* **158**, 32–36 (2020).
5. Gao, N., Śliz, M., Quan, C., Bieniek, A. & Magdziarz, A. Biomass CO_2 gasification with CaO looping for syngas production in a fixed-bed reactor. *Renew. Energy* **167**, 652–661 (2021).
6. Kenarsari, S. D. *et al.* Review of recent advances in carbon dioxide separation and capture. *RSC Adv.* **3**, 22739–22773 (2013).
7. Wang, X., Zhang, F. & Lipiński, W. Research progress and challenges in hydrate-based carbon dioxide capture applications. *Appl. Energy* **269**, 114928 (2020).
8. Circone, S., Kirby, S., Pinkston, J. C. & Stern, L. A. Measurement of gas yields and flow rates using a custom flowmeter. *Rev. Sci. Instrum.* **72**, 2709–2716 (2001).
9. Mimachi, H. *et al.* Effect of long-term storage and thermal history on the gas content of natural gas hydrate pellets under ambient pressure. *Energy Fuels* **29**, 4827–4834 (2015).
10. Nakajima, T., Akatsu, S., Ohmura, R., Takeya, S. & Mori, Y. H. Molecular storage of ozone in a clathrate hydrate formed from an O_3+O_2+CO_2 gas mixture. *Angew. Chem. Int. Ed.* **50**, 10340–10343 (2011).
11. Ricaurte, M., Dicharry, C., Renaud, X. & Torré, J. Combination of surfactants and organic compounds for boosting CO_2 separation from natural gas by clathrate hydrate formation. *Fuel* **122**, 206–217 (2014).
12. Tomita, S., Akatsu, S. & Ohmura, R. Experiments and thermodynamic simulations for continuous separation of CO_2 from CH_4 + CO_2 gas mixture utilizing hydrate formation. *Appl. Energy* **146**, 104–110 (2015).
13. Wang, B., Jin, H. & Zheng, D. Recovery of CO_2 with MEA and K_2CO_3 absorption in the IGCC system. *Int. J. Energy Res.* **28**, 521–535 (2004).
14. Gao, J., Gao, L., Dong, H., Zhang, X. & Zhang, S. Ionic liquids tailored amine aqueous solution for pre-combustion CO_2 capture: Role of imidazolium-based ionic liquids. *Appl. Energy* **154**, 771–780 (2015).
15. Merkel, T. C., Zhou, M. & Baker, R. W. Carbon dioxide capture with membranes at an IGCC power plant. *J. Membr. Sci.* **389**, 441–450 (2012).
16. Franz, J., Maas, P. & Scherer, V. Economic evaluation of pre-combustion CO_2-capture in IGCC power plants by porous ceramic membranes. *Appl. Energy* **130**, 532–542 (2014).
17. Kiyokawa, H., Horii, S., Alavi, S. & Ohmura, R. Improvement of continuous hydrate-based CO_2 separation by forming structure II hydrate in the system of H_2 + CO_2 + H_2O + Tetrahydropyran (THP). *Fuel* **278**, 118330 (2020).
18. Linga, P., Kumar, R. & Englezos, P. Gas hydrate formation from hydrogen/carbon dioxide and nitrogen/carbon dioxide gas mixtures. *Chem. Eng. Sci.* **62**, 4268–4276 (2007).
19. Cai, J., Zhang, Y., Xu, Z. M., Chen, Z. Y. & Li, X. S. Raman spectroscopic studies on carbon dioxide separation from fuel gas via clathrate hydrate in the presence of tetrahydrofuran. *Appl. Energy* **214**, 92–102 (2018).
20. Horii, S. & Ohmura, R. Continuous separation of CO_2 from a H_2 + CO_2 gas mixture using clathrate hydrate. *Appl. Energy* **225**, 78–84 (2018).
21. Ohmura, R., Shigetomi, T. & Mori, Y. H. Formation, growth and dissociation of clathrate hydrate crystals in liquid water in contact with a hydrophobic hydrate-forming liquid. *J. Cryst. Growth* **196**, 164–173 (1999).
22. Servio, P. & Englezos, P. Morphology study of structure H hydrate formation from water droplets. *Cryst. Growth Des.* **3**, 61–66 (2003).
23. Lee, J. D., Song, M., Susilo, R. & Englezos, P. Dynamics of methane-propane clathrate hydrate crystal growth from liquid water with or without the presence of *n*-heptane. *Cryst. Growth Des.* **6**, 1428–1439 (2006).
24. Sakemoto, R., Sakamoto, H., Shiraiwa, K., Ohmura, R. & Uchida, T. Clathrate hydrate crystal growth at the seawater/hydrophobic–guest–liquid interface. *Cryst. Growth Des.* **10**, 1296–1300 (2010).
25. Matsuura, R., Horii, S., Alavi, S. & Ohmura, R. Diversity in crystal growth dynamics and crystal morphology of structure-H hydrate. *Cryst. Growth Des.* **19**, 6398–6904 (2019).
26. Darbouret, M., Cournil, M. & Herri, J. M. Rheological study of TBAB hydrate slurries as secondary two-phase refrigerants. *Int. J. Refrig.* **28**, 663–671 (2005).
27. Ohmura, R. *et al.* Clathrate hydrate crystal growth in liquid water saturated with a hydrate-forming substance: variations in crystal morphology. *Philos. Mag.* **84**, 1–16 (2004).
28. Ueno, H., Akiba, H., Akatsu, S. & Ohmura, R. Crystal growth of clathrate hydrates formed with methane + carbon dioxide mixed gas at the gas/liquid interface and in liquid water. *New J. Chem.* **39**, 8254–8262 (2015).
29. Akiba, H., Ueno, H. & Ohmura, R. Crystal growth of ionic semiclathrate hydrate formed at the interface between CO_2 gas and tetra-*n*-butylammonium bromide aqueous solution. *Cryst. Growth Des.* **15**, 3963–3968 (2015).
30. Ozawa, K. & Ohmura, R. Crystal growth of clathrate hydrate with methane plus partially water soluble large-molecule guest compound. *Cryst. Growth Des.* **19**, 1689–1694 (2019).
31. Stephenson, R. M. Mutual solubilities: water-ketones, water-ethers, and water-gasoline-alcohols. *J. Chem. Eng. Data* **37**(1), 80–95 (1992).
32. Ida, H. & Kohda, K. Highly efficient natural gas hydrate production technology. *JFE Tech. Rep.* **6**, 76–80 (2004).
33. Makogon, T. Y., Larsen, R., Knight, C. A. & Sloan, E. D. Jr. Melt growth of tetrahydrofuran clathrate hydrate and its inhibition: method and first results. *J. Cryst. Growth* **179**, 258–262 (1997).
34. Smelik, E. A. & King, H. E. Jr. Crystal-growth studies of natural gas clathrate hydrates using a pressurized optical cell. *Am. Mineral.* **82**, 88–98 (1997).
35. Larsen, R., Knight, C. A. & Sloan, E. D. Jr. Clathrate hydrate growth and inhibition. *Fluid Phase Equilib.* **150–151**, 353–360 (1998).
36. Knight, C. A. & Rider, K. Free-growth forms of tetrahydrofuran clathrate hydrate crystals from the melt: plates and needles from a fast-growing vicinal cubic crystal. *Philos. Mag. A* **82**, 1609–1632 (2002).
37. Kodera, M., Takeya, S., Lassiège, M., Alavi, S. & Ohmura, R. Characterization of clathrate hydrate formed in H_2 + CO_2 + tetrahydropyran + water system as carbon capture materials. *Fuel* **295**, 120593 (2021).
38. Delroisse, H., Torré, J.-P. & Dicharry, C. Effect of a hydrophilic cationic surfactant on cyclopentane hydrate crystal growth at the water/cyclopentane interface. *Cryst. Growth Des.* **17**(10), 5098–5107 (2017).

Acknowledgements
This study was supported by a Keirin-racing-based research-promotion fund from the JKA Foundation (2020M-195) and by JSPS KAKENHI (Grant No. 17H03122). We are grateful to Masamichi Kodera, who helped us a lot with the experimental work.

Author contributions
M.M. and R.M. performed the experiments. M.M. wrote the manuscript. R.O. designed the experiments. All authors analyzed the experimental data, contributed to the scientific discussions, and reviewed the manuscript.

Competing interests
The authors declare no competing interests.

Additional information
Supplementary Information The online version contains supplementary material available at https://doi.org/10.1038/s41598-021-90802-6.

Correspondence and requests for materials should be addressed to R.O.

Reprints and permissions information is available at www.nature.com/reprints.

Publisher's note Springer Nature remains neutral with regard to jurisdictional claims in published maps and institutional affiliations.